Korean J. Chem. Eng., 37(2), 332-340 (2020)
DOI: 10.1007/s11814-019-0439-z

pISSN: 0256-1115
eISSN: 1975-7220

Measurement and correlation of phase equilibria in aqueous two-phase systems containing ionic liquid ([EOMiM]Br) and potassium citrate/ammonium citrate/potassium tartrate at different temperatures

Dongdong Wang*,, Yang Lu*,**,†, Zhuo Sun*,**, Wei Liang*,**, Dongshu Sun*, Changli Qi*, ChengZhuo Sheng*, and Xiaopeng Yu**,†**

*Key Laboratory of Preparation and Application of Environmental Friendly Materials, Jilin Normal University, Ministry of Education, Changchun, 130103, China
**Jilin Provincial Key Laboratory for Numerical Simulation, Jilin Normal University, 1301 Haifeng Street, Siping, 136000, China
(*Received 12 July 2019 • accepted 24 November 2019*)

Abstract−An aqueous two-phase system (ATPS) containing an ionic liquid (1-(2-methoxyethyl)-3-methylimidazolium bromide) and three organic salts ($K_3C_6H_5O_7$, $(NH_4)_3C_6H_5O_7$, and $K_2C_4H_4O_6$) at different temperatures was designed. Binodal data were correlated using two empirical equations, and tie-line data were fit with the utilization of Bancroft and Othmer-Tobias equations. In the systems investigated, three conclusions were drawn from the study of the phase-forming ability of salt through effective excluded volume, Gibbs free energy of ions, and the phase diagram. First, if the same cations of salt were present, the ability of salt to form phases increased with increasing valence of the anion. Second, the larger the effective excluded volume, the stronger the aforementioned ability of salt in forming phases. Third, salt had more ability to form phases if cations (or anions) contained in the salt possessed higher negative Gibbs free energy when the cation (anion) of the salt was the same. The effect of temperature on ATPSs was also investigated. It was found that it was easier to form ATPSs at lower temperature, and the tie-line slope showed growing absolute values as the temperature was decreased.

Keywords: Aqueous Two-phase System, [EOMiM]Br, Inorganic Salt, The EEV Model, Liquid-liquid Equilibrium

INTRODUCTION

An aqueous two-phase system (ATPS), as an environmentally-friendly technology used in separation and enrichment, has broad prospects for application and may add value because of its advantages, such as its being time-saving, simple, efficient, and eco-friendly [1-5]. At first the phase-forming materials of ATPS were two types of polymer [6,7], and then one polymer was replaced with a suitable salt to reduce the viscosity of ATPS, namely, polymer-salt ATPS [8,9]. Ionic liquid (IL) consisting of a specific organic cation and inorganic anion, also known as temperature molten salt, is the molten salt system that is liquid at or near room temperature. As a new green solvent, ionic liquids are widely used in extraction and separation processes because of their extremely low volatility, good thermal stability and chemical stability, high solubility and outstanding designability. Ionic liquid was introduced into the ATPS to replace polymer-salt ATPS in 2002, and ionic liquid ATPS (IL-ATPS) was born [10,11]. IL-ATPS synthesizes the advantages both of IL and ATPS: it has a shorter phase-forming time, low viscosity, no emulsification, and is reusable as an IL. Therefore, IL-ATPS has wide applications in analytical chemistry, the separation of biologic media and natural products.

The liquid-liquid equilibria data form the basis for operating and designing of IL-ATPS extraction. To date, research into the phase equilibrium of IL-ATPS has been reported, but there have been few studies on the data pertaining to phase diagrams of IL-ATPS containing salt and 1-(2-methoxyethyl)-3-methylimidazolium bromide ([EOMiM]Br). The data of phase diagrams of the IL-ATPSs containing [EOMiM]Br together with three inorganic salts (K_3PO_4, K_2CO_3, and K_2HPO_4) have been reported by our group [12]. The research reported the compositions of the liquid-liquid equilibrium of the IL-ATPSs consisting of [EOMiM]Br and three organic salts ($K_3C_6H_5O_7$, $K_2C_4H_4O_6$, and $(NH_4)_3C_6H_5O_7$), and discussed the influence of all aspects thereof.

EXPERIMENTAL WORK

1. Materials

Analytical grade reagents (GR, min. 99% by mass fraction) organic salts ($K_3C_6H_5O_7$, $(NH_4)_3C_6H_5O_7$, and $K_2C_4H_4O_6$) were supplied by the Sinopharm Chemical Reagent Co., Ltd., Shanghai, China. Ionic liquid [EOMiM]Br of purity quoted above exceeding 0.99 mass fraction was purchased from Chengjie Chemical Co., Ltd., Shanghai, China. Standard samples (solasonine, solamargine, ciprofloxacin, lomefloxacin, thiamphenicol, sulfadiazine, and sulfamethazine) with over 99% purity were purchased from the Chinese National

†To whom correspondence should be addressed.
E-mail: luyang33@126.com, yyxxpp@jlnu.edu.cn

Institute for the Control of Pharmaceutical and Biological Products (Beijing, China). The solutions used in the research were prepared with double-distilled deionized water. All reagents were directly utilized without further purification.

2. Apparatus and Procedure

Binodal curves were obtained by use of the following titration method: we poured, into a 50-mL vessel, an ionic liquid ([EOMiM]Br) solution with known concentration, with the system temperature constrained to be within a required range of temperatures by covering the vessel with a jacket. A DC-2008 water thermostat (Shanghai Hengping Instrument Factory, China) was used to regulate the water temperature. The solution turned cloudy after adding a proper salt solution drop-by-drop, evincing the formation of two liquid phases. We computed mass fractions of [EOMiM]Br and the salts after weighing with a BS124S analytical balance with an uncertainty of $\pm 1.0\times10^{-7}$ kg (Beijing Sartorius Instrument Co., China). This was followed by the addition of a drop of water to clarify the solution, and the aforementioned steps were then repeated.

By mixing proper quantities of water, [EOMiM]Br, and salts in the vessel, we determined data pertaining to tie-lines from a series of ATPSs. Then, the vessel was placed in the thermostatic water-bath for more than 5 h to separate the solution therein into two phases. The thermostatic bath was maintained at the set temperature ±0.05 °C. A UV-2450 UV-Vis spectrometer (Shimadzu Corporation, Japan) was used to measure concentrations of [EOMiM]Br in the two phases by UV absorbance of $[EOMiM]^+$ [13-16]. 1 g solution taken from top phase or bottom phase was added to a 100-mL volumetric flask, and then water was added to volume. This solution was recorded as Solution A. 1 mL of Solution A was transferred into another 100-mL volumetric flask, and then water was added to the volume. This solution was recorded as Solution B. The UV absorbance of $[EOMiM]^+$ in Solution B was measured by UV-Vis spectrometer at 218 nm. The formula for the standard curve of [EOMiM]Br is as follows:

$$c=61.9694*Abs-1.0720\ (R=0.9998) \quad (1)$$

where c is the concentration of [EOMiM]Br (0 mg·L^{-1} to 80 mg·L^{-1}), and Abs is the UV absorbance. Mass fractions of [EOMiM]Br display a measurement uncertainty of ±0.001. The concentrations of salts ($K_3C_6H_5O_7$ and $K_2C_4H_4O_6$) in two phases were determined by the TAS-968 atomic absorption spectrophotometer (Beijing Purkinje General Instrument Co., Ltd., China), while that of $(NH_4)_3C_6H_5O_7$ was measured by adopting a conductivity measuring device (model DDSJ-308A, Shanghai Precision & Scientific Instrument Co., Ltd., China). The water content was measured by mass balance. The concentration of $(NH_4)_3C_6H_5O_7$ was determined by conductivity at 298.15 K. Since the samples contained [EOMiM]Br that is electrically conductive, a dual equation was used to determine the concentration of $(NH_4)_3C_6H_5O_7$. This method was inspired by the method of measurement of polymer concentration by refractive index [17,18]. The relationship between conductivity σ, and the mass fractions of $(NH_4)_3C_6H_5O_7$, w_1, and [EOMiM]Br, w_2 is given by

$$\sigma=\sigma_0+a_1w_1+a_2w_2 \quad (2)$$

where σ_0, a_1, and a_2 are constants. For the [EOMiM]Br-$(NH_4)_3C_6H_5O_7$ system, coefficients σ_0, a_1, and a_2 were −0.0199, 1236.15, and 459.44, respectively. Note that this equation is only valid for mass fractions $w_1\leq0.25\%$ and $w_2\leq0.30\%$. Therefore, it was necessary to dilute the samples to the aforementioned mass fraction range before conductivity was measured. Mass fractions of salts ($K_3C_6H_5O_7$ and $K_2C_4H_4O_6$) showed a precision higher than ±0.0001. The measuring precision for mass fraction of $(NH_4)_3C_6H_5O_7$ is higher than ±0.002 (the uncertainty calculation method is given in Supplementary Materials).

The tie-line length (TLL) and the tie-line slope (S) for the system with disparate components were separately calculated thus:

$$TLL=[(w_1^t-w_1^b)^2+(w_2^t-w_2^b)^2]^{0.5} \quad (3)$$

$$S=(w_1^t-w_1^b)/(w_2^t-w_2^b) \quad (4)$$

where w_1^t represents the mass fraction of [EOMiM]Br (1) in the phase in the top of the solution, w_2^t denotes that of salt (2) in this phase, w_1^b refers to mass fraction of [EOMiM]Br (1) in the phase at the bottom of the solution, and w_2^b represents that of salt (2) in the phase at the bottom.

Table 1. Binodal data for the [EOMiM]Br(1)+$K_3C_6H_5O_7$(2)+H_2O(3) ATPSs at 288.15, 298.15, and 308.15 K[a]

T=288.15 K		T=298.15 K		T=308.15 K	
$100w_1$	$100w_2$	$100w_1$	$100w_2$	$100w_1$	$100w_2$
59.88	0.38	60.06	0.51	61.08	0.59
57.28	0.99	57.96	1.21	59.30	1.61
56.34	1.42	56.86	1.73	57.20	2.48
54.18	2.18	56.07	2.14	56.45	2.61
52.73	2.91	54.45	2.94	55.35	3.06
50.88	3.83	52.08	3.83	54.01	3.60
49.57	4.49	51.23	4.26	52.87	3.93
48.00	5.09	49.10	4.98	50.71	4.84
46.97	5.69	48.21	5.37	49.43	5.42
45.64	6.19	47.66	5.72	47.97	6.08
44.07	6.95	47.21	6.04	46.35	6.68
42.54	7.58	45.66	6.75	44.42	7.55
41.44	8.15	43.38	7.76	42.87	8.33
39.92	8.85	42.08	8.41	41.42	9.05
38.52	9.56	41.02	9.04	40.73	9.53
37.94	10.05	40.07	9.43	39.56	10.03
36.90	10.68	38.21	10.56	37.23	11.34
34.85	11.85	36.57	11.45	35.72	12.32
34.28	12.13	34.89	12.66	34.38	13.46
33.51	12.83	33.82	13.58	32.68	14.56
32.27	13.46	32.91	14.13	31.18	15.63
31.77	13.88	31.23	15.12	29.10	17.13
29.55	15.23	30.06	15.98	27.98	17.93
28.46	16.15	29.06	16.86	27.08	19.04
27.57	16.82	28.09	17.49	25.38	21.01
26.15	17.66	26.78	18.53	23.81	23.43
25.13	18.94	25.23	19.67	22.50	25.08
23.24	21.04	24.01	20.99		

[a]Standard uncertainties u are u(w)=0.0001, u(T)=0.05 K, and u(p)=10 kPa

Table 2. Binodal data for the [EOMiM]Br(1)+$(NH_4)_3C_6H_5O_7$/$K_2C_4H_4O_6$(2)+H_2O(3) ATPSs at 308.15 K[a]

[EOMiM]Br-$(NH_4)_3C_6H_5O_7$ ATPS				[EOMiM]Br-$K_2C_4H_4O_6$ ATPS			
$100w_1$	$100w_2$	$100w_1$	$100w_2$	$100w_1$	$100w_2$	$100w_1$	$100w_2$
65.67	5.20	34.77	24.94	68.87	2.14	36.17	18.21
60.74	7.09	31.96	27.15	67.77	2.27	35.13	18.99
59.45	7.53	31.24	27.79	64.23	3.43	32.97	20.55
56.90	9.06	30.26	28.70	63.16	3.82	29.73	22.94
56.55	9.31	29.95	29.18	62.25	4.11	26.51	25.48
53.48	10.81	28.40	30.18	60.18	4.97	25.26	26.01
53.16	10.95	28.39	30.25	59.13	5.43	23.19	28.22
52.26	11.43	25.55	32.74	56.30	6.47	20.88	30.95
48.67	14.00	25.70	32.75	55.45	6.78	19.98	31.26
47.66	14.98	25.93	32.76	53.11	7.66	16.57	34.17
44.68	16.68	25.57	32.83	50.51	8.86	13.18	38.92
43.27	18.12	22.50	35.71	48.47	9.98		
41.43	19.68	22.20	36.20	46.63	10.95		
40.38	20.41	18.03	40.69	43.47	13.29		
39.10	21.31	17.75	41.18	43.43	13.31		
39.10	21.38			42.10	14.02		
35.58	24.02			39.05	16.12		

[a]Standard uncertainties u are u(w)=0.0001, u(T)=0.05 K, and u(p)=10 kPa

RESULTS AND DISCUSSION

1. Binodal Data and Correlation

We determined binodal data for [EOMiM]Br-$K_3C_6H_5O_7$ in the IL-ATPS at different temperatures (288.15, 298.15, and 308.15 K) (Table 1), and reported binodal data on IL-ATPS containing [EOMiM]Br and salts ($(NH_4)_3C_6H_5O_7$ and $K_2C_4H_4O_6$) at 308.15 K (Table 2). For the IL-ATPSs studied in the present work, the binodal curves are illustrated in Figs. 1 and 2. In existing studies of phase equilibrium of ATPS, many empirical equations are used to compute correlations in binodal data, thus attaining the expected effects. The current research obtained correlation of binodal data on the systems of interest by using current empirical equations, and demonstrated favorable correlations between Eqs. (5) and (6):

$$w_1 = \exp(a + bw_2^{0.5} + cw_2 + dw_2^2) \quad (5)$$

$$w_1 = aw_2^3 + bw_2^2 + cw_2 + d \quad (6)$$

where, w_1 represents the mass fraction of [EOMiM]Br, while w_2 denotes that of salts; a, b, c, and d are fitting parameters. The binodal data of micromolecular and organic solvents-salt ATPSs [19,20] and polymer-salt ATPSs [21,22] are correlated using Eq. (6). Binodal data for polymer-salt ATPSs were fitted using the third-order polynomial equation (Eq. (5)) [23], as well as ionic liquid-salt ATPSs [24, 25]. For the systems studied here, fitting parameters a, b, c, and d in Eqs. (5) and (6) were determined by regression analysis of binodal data in Tables 1 and 2 and are listed in Tables 3 and 4, respectively.

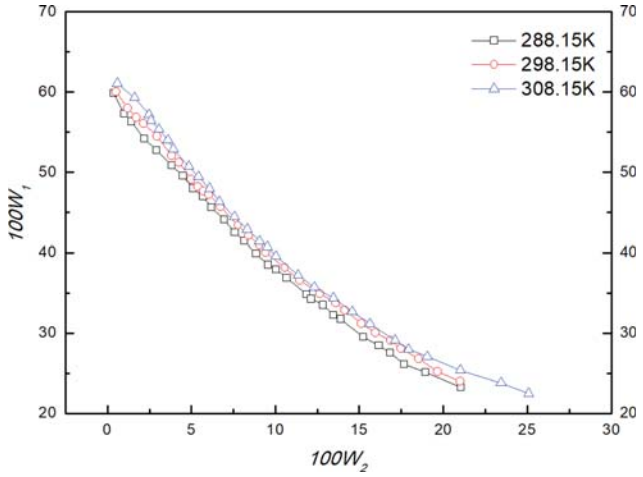

Fig. 1. Binodal curves plotted for the IL ([EOMiM]Br)(1)+$K_3C_6H_5O_7$ (2)+H_2O(3) ATPSs at 288.15, 298.15, and 308.15 K.

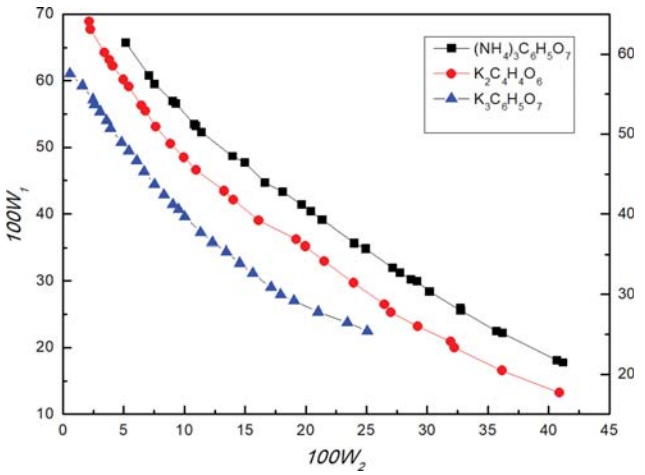

Fig. 2. Binodal curves plotted for the IL ([EOMiM]Br)(1)+$(NH_4)_3C_6H_5O_7$/$K_2C_4H_4O_6$/ $K_3C_6H_5O_7$(2)+H_2O(3) ATPSs at 308.15 K.

Table 3. Values of parameters of Eq. (5) for [EOMiM]Br(1)+$K_3C_6H_5O_7$/$C_6H_5O_7(NH_4)_3$/$C_4H_4O_6K_2$(2)+H_2O(3) ATPSs

T (K)	a	b	c	d	R^2	100SD[a]
[EOMiM]Br(1)+$K_3C_6H_5O_7$(2)+H_2O(3)						
288.15	−0.5075	0.0555	−4.7736	0.0748	0.9992	0.28
298.15	−0.4985	0.1715	−4.9966	0.9972	0.9996	0.20
308.15	−0.5074	0.7764	−7.3941	7.6370	0.9997	0.18
[EOMiM]Br(1)+$C_6H_5O_7(NH_4)_3$(2)+H_2O(3)						
308.15	0.1690	−3.3092	3.5261	−7.3251	0.9998	0.20
[EOMiM]Br(1)+$C_4H_4O_6K_2$(2)+H_2O(3)						
308.15	−0.1019	−1.9114	0.5533	−6.2592	0.9995	0.36

[a]$SD=(\Sigma_{i=1}^{n}(w_1^{cal}-w_1^{exp})^2/N)^{0.5}$ where w_1^{exp} is the experimental mass fraction of [EOMiM]Br in Tables 1 and 2, w_1^{cal} refers to the corresponding data calculated using Eq. (5); N represents the number of binodal data points.

Table 4. Values of parameters of Eq. (6) for [EOMiM]Br(1)+$K_3C_6H_5O_7$/$C_6H_5O_7(NH_4)_3$/$C_4H_4O_6K_2$(2)+H_2O(3) ATPSs

T (K)	a	b	c	d	R^2	100SD[a]
[EOMiM]Br(1)+$K_3C_6H_5O_7$(2)+H_2O(3)						
288.15	1.5197	3.6270	−2.5915	0.6016	0.9994	0.25
298.15	−5.2089	−5.5229	−2.7183	0.6152	0.9996	0.20
308.15	−2.3759	5.7825	−2.9316	0.6359	0.9995	0.26
[EOMiM]Br(1)+$C_6H_5O_7(NH_4)_3$(2)+H_2O(3)						
308.15	−3.4716	3.770264	−2.3861	0.7586	0.9990	0.41
[EOMiM]Br(1)+$C_4H_4O_6K_2$(2)+H_2O(3)						
308.15	−6.9442	6.5445	−3.0806	0.7403	0.9987	0.57

[a]$SD=(\Sigma_{i=1}^{n}(w_1^{cal}-w_1^{exp})^2/N)^{0.5}$ where w_1^{exp} is the experimental mass fraction of [EOMiM]Br in Tables 1 and 2, w_1^{cal} denotes the corresponding data calculated using Eq. (6); N represents the number of binodal data points.

Tables 3 and 4 also report square of correlation coefficients (R^2), as well as the corresponding standard deviation (SD). To examine the fitting precision and extrapolation performance of these two equations, those data not shown in Tables 1 and 2 were used to calculate the SD. These data and SD are given in Supplementary Material (Tables S1 and S2). From the values of R^2 and SD in Tables 3 and 4, and Supplementary Tables S1 and S2, it can be seen that these two equations are capable of ideally fitting binodal data from the sys-

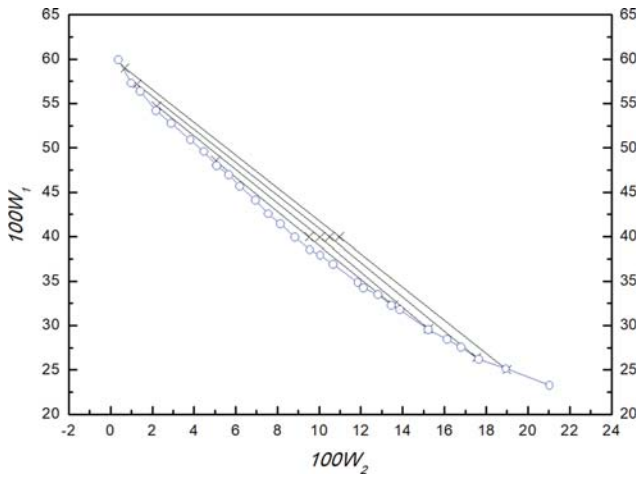

Fig. 3. Binodal curves and tie-line for the [EOMiM]Br(1)+$K_3C_6H_5O_7$(2)+H_2O(3) ATPS at 288.15 K; ×, tie-line; ○, binodal curves.

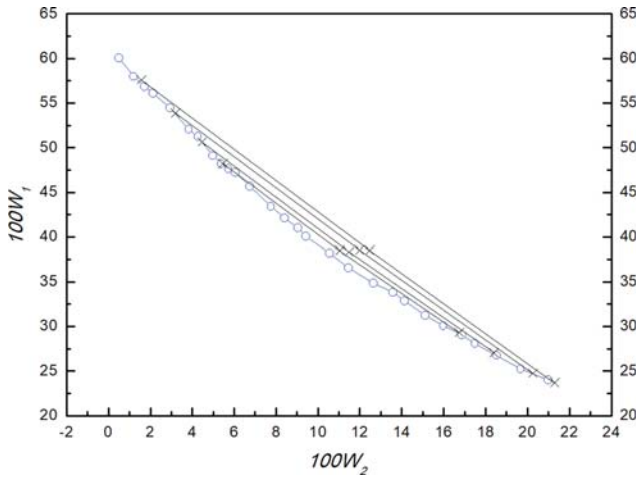

Fig. 4. Binodal curves and tie-line for the [EOMiM]Br(1)+$K_3C_6H_5O_7$(2)+H_2O(3) ATPS at 298.15 K; ×, tie-line; ○, binodal curves.

Table 5. Tie-line data for the [EOMiM]Br(1)+$K_3C_6H_5O_7$/$C_6H_5O_7(NH_4)_3$/$C_4H_4O_6K_2$(2)+H_2O(3) ILATPSs[a]

T (K)	Total system		Top phase		Bottom phase		TLL	S
	$100w_1$	$100w_2$	$100w_1^t$	$100w_2^t$	$100w_1^b$	$100w_2^b$		
[EOMiM]Br(1)+$K_3C_6H_5O_7$(2)+water(3)								
288.15	39.93	9.51	48.54	5.05	32.31	13.53	18.31	−1.9142
288.15	39.91	10.03	54.73	2.21	29.65	15.23	28.26	−1.9238
288.15	39.97	10.49	57.17	1.25	26.41	17.53	34.80	−1.8880
288.15	39.95	10.96	58.99	0.67	25.03	18.99	38.59	−1.8536
298.15	38.51	11.03	48.24	5.45	29.33	16.43	22.02	−1.6762
298.15	38.36	11.48	50.63	4.46	27.06	18.39	27.38	−1.6922
298.15	38.55	11.98	53.89	3.19	24.76	20.24	33.75	−1.7089
298.15	38.51	12.47	57.61	1.56	23.68	21.29	39.25	−1.7209
308.15	35.73	13.00	43.79	8.02	27.27	18.57	19.60	−1.5650
308.15	35.69	13.50	47.45	6.39	26.61	19.47	24.60	−1.5652
308.15	35.57	14.02	50.95	4.68	25.05	21.27	30.76	−1.5652
308.15	35.64	14.58	53.24	3.88	24.83	21.92	33.65	−1.5799
[EOMiM]Br(1)+$(NH_4)_3C_6H_5O_7$(2)+water(3)								
308.15	41.06	20.55	51.81	12.06	25.86	32.67	33.14	−1.2588
308.15	42.03	20.51	55.48	10.01	22.86	35.63	41.48	−1.2729
308.15	43.07	20.53	58.99	7.98	19.79	38.71	49.81	−1.2760
308.15	44.05	20.51	62.17	6.26	17.93	40.89	56.18	−1.2778
[EOMiM]Br(1)+$K_2C_4H_4O_6$(2)+water(3)								
308.15	40.02	16.23	48.27	10.08	32.08	21.95	20.08	−1.3637
308.15	41.00	16.26	52.38	7.76	28.88	24.76	29.00	−1.3824
308.15	42.03	16.31	55.98	6.38	23.41	29.03	39.67	−1.4392
308.15	43.09	16.29	58.86	5.12	20.88	31.72	46.37	−1.4285

[a]Standard uncertainties u are u(w)=0.0001, u(T)=0.05 K, and u(p)=10 kPa.

tems studied.

2. Liquid-liquid Equilibrium Data and Correlation

We determined tie-line data of [EOMiM]Br-$K_3C_6H_5O_7$ IL-ATPS at 288.15, 298.15, and 308.15 K (Table 5), in which tie-line data on IL-ATPS containing [EOMiM]Br and salts ($(NH_4)_3C_6H_5O_7$ and $K_2C_4H_4O_6$) determined at 308.15 K are also given. The TLL and the tie-line slope (S) in Table 5 were calculated by using Eqs. (1) and (2). Figs. 3 to 7 depict tie-line and binodal curves of studied IL-ATPSs at each temperature. Tie-lines data were fitted by the widely used Bancroft and Othmer-Tobias [26] Eqs. (5) and (6) that were applied to the correlation of liquid-liquid equilibria data from many systems [24,27,28].

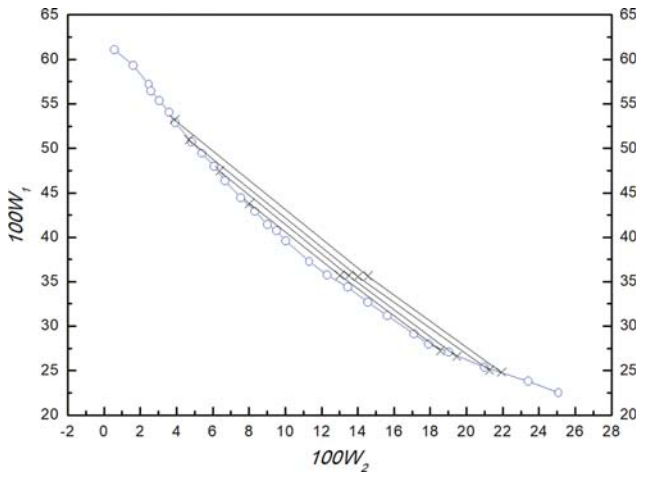

Fig. 5. Binodal curves and tie-line for the [EOMiM]Br(1)+$K_3C_6H_5O_7$(2)+H_2O(3) ATPS at 308.15 K; ×, tie-line; ○, binodal curves.

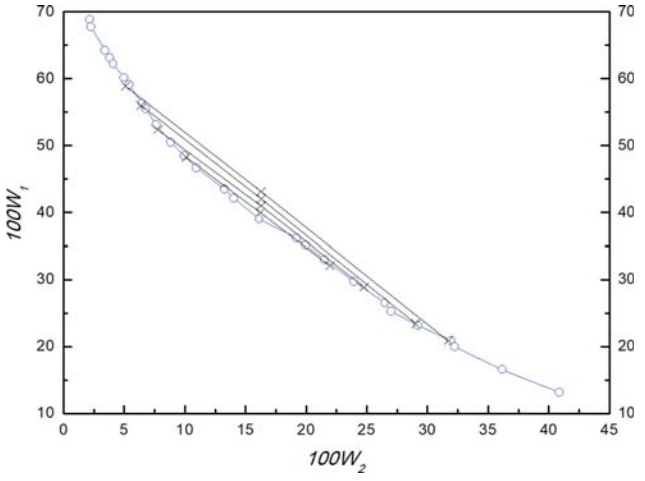

Fig. 6. Binodal curves and tie-line for the [EOMiM]Br(1)+$K_2C_4H_4O_6$(2)+H_2O(3) ATPS at 308.15 K; ×, tie-line; ○, binodal curves.

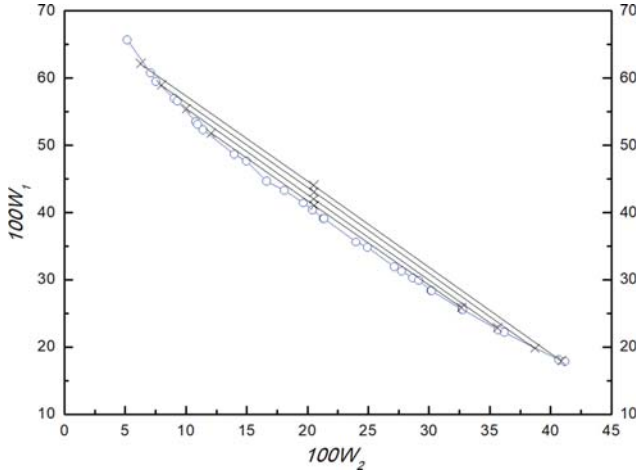

Fig. 7. Binodal curves and tie-line for the [EOMiM]Br(1)+$(NH_4)_3C_6H_5O_7$(2)+H_2O(3) ATPS at 308.15 K; ×, tie-line; ○, binodal curves.

$$\left(\frac{1-w_1^t}{w_1^t}\right)=k_1\left(\frac{1-w_2^b}{w_2^b}\right)^n \tag{7}$$

$$\left(\frac{w_3^b}{w_2^b}\right)=k_2\left(\frac{w_3^t}{w_1^t}\right)^r \tag{8}$$

where, w_1^t represents mass fractions of [EOMiM]Br in the phase in the top of the solution, w_2^b is that of salt in the bottom, w_3^t and w_2^b denote mass fractions of water in phases in top and bottom of the solution; k_1, k_2, n, and r are fitting parameters (Table 6). For the systems investigated here, R^2 and SD are also listed (Table 6).

3. Effect of the Salt Type on the Binodal Curves

Our previous studies [29-31] found that the salt type affects the equilibrium of two liquid phases for polymer-salt ATPSs. In the present work, the ability of salts to form phases was investigated in three ways: first, binodal curves of the ATPS carrying [EOMiM]Br, together with salts ($K_3C_6H_5O_7$, $(NH_4)_3C_6H_5O_7$, and $K_2C_4H_4O_6$) at 308.15 K are shown in Fig. 8, which also illustrates the previously reported binodal curves of the ATPS with [EOMiM]Br and three salts (K_3PO_4, K_2HPO_4, and K_2CO_3) [12]. For the purpose of making the molecular relationship clearer for the systems investigated herein [32,33], the concentrations of two materials ([EOMiM]Br and salts) in Fig. 8 are displayed as molality fraction (w_1/M_1 and w_2/M_2). As seen from Fig. 8, the ability of salts to form phases was enhanced as the valence of the anions increased for a given valence of the cations. For the five types of salt studied here, they have the same cation (K^+), and then the phase-forming abilities of salts containing a trivalent anion is stronger than that of salts with a bivalent anion, namely, trivalent potassium salts (K_3PO_4>$K_3C_6H_5O_7$)>bivalent potassium salts (K_2HPO_4>K_2CO_3>$K_2C_4H_4O_6$). For those salts consisting of the same cation and an anion of the same valence, what governs their phase-forming abilities? We will present two aspects to this question below.

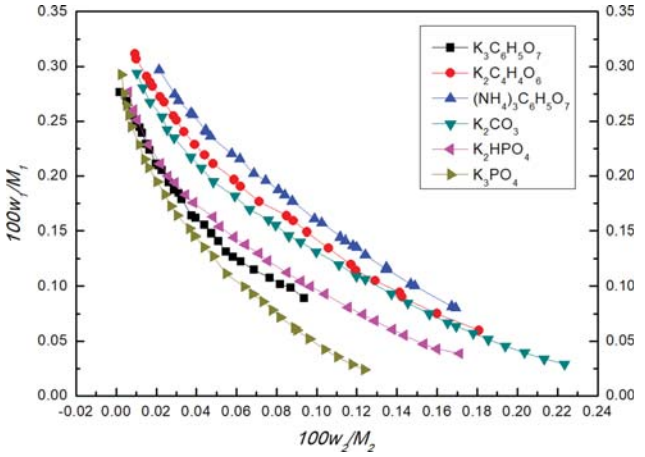

Fig. 8. Effect of type of salt on the binodal curves plotted in molality fraction for the ATPSs at 308.15 K.

The first is EEV, the effective excluded volume [34]. The EEV model was built with binodal model for two polymers ATPSs based on statistical geometry methods, and then utilized for correlation of binodal data on other type ATPSs. The EEV model was applied to analysis of the [EOMiM]Br ATPSs, and the corresponding equations are:

$$\ln\left(V_{213}^*\frac{w_2}{m_2}+f_{213}\right)+V_{213}^*\frac{w_1}{m_1}=0 \tag{9}$$

Table 6. Tie-line of values of parameters of Eqs. (7) and (8) for the [EOMiM]Br(1)+$K_3C_6H_5O_7$/$C_6H_5O_7(NH_4)_3$/$C_4H_4O_6K_2$(2)+H_2O(3) ILATPSs

T (K)	k_1	n	k_2	r	R_1^2	R_2^2	$100SD^1$	$100SD^2$
[EOMiM]Br(1)+$K_3C_6H_5O_7$(2)+water(3)								
288.15	161.5	0.9908	4.256	0.8914	0.9070	0.9016	4.0	3.2
298.15	155.7	1.216	3.271	0.8269	0.9320	0.9494	2.1	2.0
308.15	101.5	1.704	2.771	0.6110	0.9702	0.9716	1.5	1.6
[EOMiM]Br(1)+$(NH_4)_3C_6H_5O_7$(2)+water(3)								
308.15	398.7	1.179	1.653	0.7365	0.9944	0.9976	0.47	0.44
[EOMiM]Br(1)+$K_2C_4H_4O_6$(2)+water(3)								
308.15	372.3	0.8345	2.435	0.9922	0.9883	0.9979	0.84	0.75

$SD=(\Sigma_{i=1}^{n}(w_1^{cal}-w_1^{exp})^2/N)^{0.5}$ where w_1^{exp} is the experimental mass fraction of [EOMiM]Br in Table 5, w_1^{cal} represents the corresponding data calculated using Eqs. (7) and (8); N represents the number of tie-line data points.

Table 7. Values of parameters of effective excluded volume (EEV) of salts using Eq. (9) for [EOMiM]Br(1)+$K_3C_6H_5O_7$/$(NH_4)_3C_6H_5O_7$/$K_2C_4H_4O_6$(2) +H_2O(3) ATPSs at different temperatures

Salt	T (K)	$V^*_{213}\cdot10^{-3}$ (g·mol^{-1})	f_{213}	R^2	100SD[a]
$K_3C_6H_5O_7$	288.15	0.7426	0.0368	0.9162	8.03
$K_3C_6H_5O_7$	298.15	0.4107	0.2659	0.9965	4.54
$K_3C_6H_5O_7$	308.15	0.4007	0.2704	0.9977	4.28
$(NH_4)_3C_6H_5O_7$	308.15	0.1027	0.5183	0.9967	4.18
$K_2C_4H_4O_6$	308.15	0.1312	0.3322	0.9932	4.96
K_3PO_4[b]	308.15	0.5942	0.1810	0.9939	0.0062
K_2HPO_4[b]	308.15	0.3028	0.4428	0.9633	0.0133
K_2CO_3[b]	308.15	0.1628	0.6317	0.9741	0.0126

[a]$SD=(\Sigma_{i=1}^{n}(w_1^{cal}-w_1^{exp})^2/N)^{0.5}$ where w_1^{exp} is the experimental mass fraction of [EOMiM]Br in Tables 1 and 2, w_1^{cal} represents the corresponding data calculated using Eq. (9); N represents the number of binodal data points.
[b]Data obtained from Reference [12].

$$\ln\left(V^*_{213}\frac{w_2}{m_2}\right)+V^*_{213}\frac{w_1}{m_1}=0 \tag{10}$$

where V^*_{213} represents the scaled EEV of salts; m_1 and w_1 are the molecular mass and mass fraction of [EOMiM]Br; molecular mass and mass fraction of salts are expressed as m_2 and w_2, respectively. After fully blending the [EOMiM]Br with salt, most molecules of the salts were tightly-packed in networks of [EOMiM]Br molecules, but a small amount of salt molecules did not enter any network, and their effective available volume fraction is represented by f_{213}. For the systems studied here, Table 7 displays V^*_{213} and f_{213}, in which the V^*_{213} and f_{213} values of ATPS containing [EOMiM]Br and salts (K_3PO_4, K_2HPO_4, K_2CO_3) at 308.15 K are also given [12]. It was found that the order of V^*_{213} is K_3PO_4>$K_3C_6H_5O_7$>K_2HPO_4>K_2CO_3>$K_2C_4H_4O_6$>$(NH_4)_3C_6H_5O_7$ for the investigated systems at 308.15 K. This agrees with the ranking of salts in phase formation terms obtained from Fig. 8. We can draw one conclusion from this: the ability of salts in phase formation is associated with V^*_{213}. A larger V^*_{213} indicates a higher ability of the salt to form phases.

Rogers [35] suggested that the Gibbs free energies in hydration of ions affects the ability of salt to form phases. As the five types of salts studied here (K_3PO_4, K_2HPO_4, K_2CO_3, $K_3C_6H_5O_7$, and $K_2C_4H_4O_6$) have the same cation, we will discuss the correlation of the phase-forming abilities of salts with Gibbs free energies of their anions. Gibbs free energies of the studied anions are expressed as follows:

$C_4H_4O_6^{2-}$ (−1,090 kJ·mol^{-1})<CO_3^{2-} (−1,315 kJ·mol^{-1})<
HPO_4^{2-} (−1,789 kJ·mol^{-1})<$C_6H_5O_7^{3-}$ (−2,763 kJ·mol^{-1})<
PO_4^{3-} (−2,765 kJ·mol^{-1})

If the Gibbs free energies of anions are more negative from the above order of Gibbs free energy of anions and the order of ability of salts to form phases in Fig. 8, the ability of salts to form phases is higher. Then, we will discuss the correlation between the abilities of salts to form phases and Gibbs free energies of their cations because two salts investigated ($K_3C_6H_5O_7$ and $(NH_4)_3C_6H_5O_7$) have the same anion, and Gibbs free energies of the studied cations are:

NH_4^+ (−285 kJ·mol^{-1})<K^+ (−295 kJ·mol^{-1})

Similarly, as is known from the Gibbs free energies of cations and the data in Fig. 8, salts containing cations with more negative Gibbs free energies can better form phases.

4. Effect of Temperature on the Binodal Curves

System temperature, a critical factor influencing the experiment, affects the phase-forming of ATPS. We measured the effects of the temperature on the ability of [EOMiM]Br ATPS in phase-formation terms. Fig. 1 shows binodal curves of [EOMiM]Br-$K_3C_6H_5O_7$ ATPS at 288.15, 298.15, and 308.15 K. As the temperature rises, the binodal curves move to the right, implying that the temperature rise will result in the areal contraction of the two phases. Thus, the rising temperature can prevent the formation of a two-phase system. This is consistent with the reported behaviour of ionic liquid-salt ATPSs [12,24,27]. In two-phase formation, mutual exclusion of a salt and an ionic liquid was found. This mainly results from their competition for the water; therefore, Zafarani-Moattar and Hamzehzadeh [36] used an excess number of water molecules adjacent to the ionic liquid pairs to explain the effect of temperature on the phase forming ability. For a given electrolyte, the excess number of water molecules and the salting-out coefficient can be expressed as follows:

$$\frac{k_s}{v}=0.018N_{ew}\frac{d(\phi c_s)}{dc_s} \tag{11}$$

where N_{ew} is the excess number of water molecules per ionic liquid particles in the salt-depleted region, k_s represents the salting-out coefficient, c_s is the molality of the salt, v represents the number of moles of ions in the fully dissociated mole of electrolyte, and ϕ is the molal osmotic coefficient. The salting-out coefficient was described by a Setschenow-type equation:

$$\ln\left(\frac{c_I^t}{c_I^b}\right)=k_I(c_I^b-c_I^t)+k_s(c_s^b-c_s^t) \tag{12}$$

where k_I and k_s are the activity coefficient of ionic related to its concentration and the salting-out coefficient, c represents the molality of the ionic liquid and salt, subscript I and s represent the ionic liquid and salt, superscript t and b represent the top phase and bottom phase. The molal osmotic coefficient was calculated by using the following equation:

Table 8. Excess number of water molecules per [EOMiM]Br pair

T/K	k_s/v (kg·mol^{-1})	$d(\phi c_s)/dc_s$	N_{ew}
288.15	0.36	0.74	27
298.15	0.34	0.73	26
308.15	0.29	0.73	22

$$\phi = \frac{\ln(a_w)}{vmM_w} \tag{13}$$

where a_w is the activity of water, M_w is the molecular weight of water, m represents the molality of salt, v is the number of moles of ions in the fully dissociated mole of electrolyte. For tripotassium citrate ATPS, the activity of water was obtained from data reported by Sadeghi et al. [37]. The values for N_{ew} along with the corresponding values for $d(\phi c_s)/dc_s$ and k_s/v are given in Table 8. The preferential hydration of [EOMiM]Br can be quantified by using N_{ew} values. From the values of N_{ew} in Table 8, the number of water molecules present increases with the decrease in temperature. Then the hydration sheath per [EOMiM]Br pair increases with the decrease in temperature. Therefore, the exclusion extent will increase because the structure-forming ions may be less accessible to the near-surface region of the [EOMiM]Br pairs. The temperature decrease is conducive to forming two-phase systems in those ATPSs studied here. This is also confirmed by EEV values in Table 7. EEV values of [EOMiM]Br-$K_3C_6H_5O_7$ ATPS decrease with the increase in temperature. This is another way to show that the extent of exclusion of ionic liquid and salt decreases with increasing temperature. On the contrary, the temperature increase is conducive to forming two-phase systems for polymer ATPSs, namely, the binodal curves of polymer ATPSs shifted leftwards with increasing temperature [38,39]. This revealed that temperature has completely different effects upon the two types of ATPSs: however, to the other ATPS, micro-molecule organic solvent ATPSs, temperature exerts a lesser effect upon the binodal curves of ATPSs [19,20,40], with the binodal curve only moving a little to the left with increasing temperature.

5. Effect of Temperature on the Tie-lines

Fig. 9 shows tie-lines of [EOMiM]Br-$K_3C_6H_5O_7$ IL-ATPS at three temperatures, and Eq. (2) expresses the tie-line slope (S). By investigating Fig. 9 and the data in Table 6, S for the IL-ATPS studied here showed increasing absolute values with the decrease in temperature. Weakening hydrophobicity of [EOMiM]Br with increasing temperature is the key cause of this phenomenon. Water moves in the phase in the top of the solution from the bottom because the hydrophilicity of [EOMiM]Br increases with the temperature. Therefore, w_1^t and w_2^t decrease, and w_1^b and w_2^b increase as the temperature rises, which causes a decreasing absolute value of ($w_1^t - w_1^b$) and an increasing absolute value of ($w_2^t - w_2^b$). Then S displays a decreasing absolute value as the temperature increases.

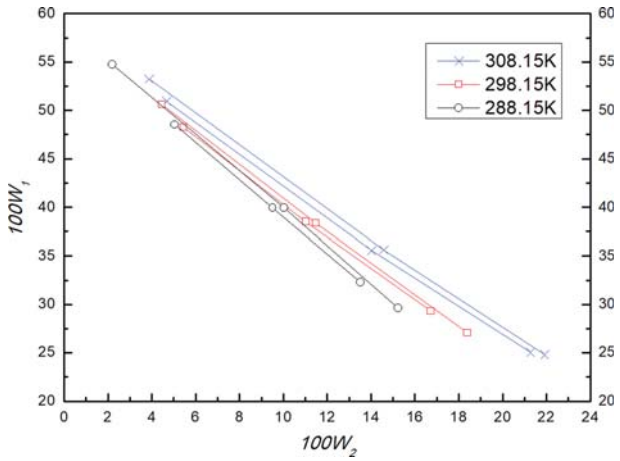

Fig. 9. Tie-line for the [EOMiM]Br(1)+$K_3C_6H_5O_7$(2)+H_2O(3) ATPS at 288.15, 298.15, and 308.15 K.

6. Extraction Efficiency and Partition Efficiency of [EOMiM]Br ATPS

For several antibiotics and alkaloids, the extraction efficiency and partition efficiency of [EOMiM]Br-$K_3C_6H_5O_7$ ATPS were investigated to test selectivity and distribution. The extraction efficiency was measured by the ratio of the mass of the object sample in the top phase to that in the initial system as follows:

$$E\,\% = \frac{C_t \times V_t}{m_s} \times 100 \tag{14}$$

where V_t is the volume of top phase, C_t is the concentration of object sample in the top phase, and m_s was the total mass of object sample in the initial system before extraction. The partition efficiency was measured by using a distribution coefficient that was the ratio of the object sample mass in the top phase to that in the bottom phase as follows:

$$F = \frac{C_t \times V_t}{C_b \times V_b} \tag{15}$$

where C is the concentration of object sample, V is the volume, and t and b represent the top phase and bottom phase. For ciprofloxacin (CIP), lomefloxacin (LOM), thiamphenicol (TAP), sulfadiazine (SD), sulfamethazine (SM2), solasonine, and solamargine, the extraction efficiencies (E%) and distribution coefficient (F) are listed in Table 9. Extraction efficiencies all exceed 90%, and the enrichment factors all exceed 9.68 (Table 9). This preliminary investigation shows that the [EOMiM]Br-$K_3C_6H_5O_7$ ATPS had good partitioning and enrichment qualities.

CONCLUSION

Binodal data and tie-line data for [EOMiM]Br-$K_3C_6H_5O_7$ IL-

Table 9. The extraction efficiency and distribution coefficient for several antibiotics and alkaloids

Object sample	Extraction efficiency (E%)	Distribution coefficient (F)
Ciprofloxacin	99.72	356.14
Lomefloxacin	97.77	43.90
Thiamphenicol	99.63	270.74
Sulfadiazine	99.31	143.51
Sulfamethazine	97.04	32.83
Solasonine	95.90	23.39
Solamargine	90.64	9.68

ATPS at 288.15, 298.15, and 308.15 K, and for [EOMiM]Br-$(NH_4)_3C_6H_5O_7$/$K_2C_4H_4O_6$ IL-ATPSs at 308.15 K, were determined. Binodal data correlated with two types of non-linear equations, and Bancroft and Othmer-Tobias equations were used to fit these tie-line data. From the phase diagram, as anion valence increased, the ability of the salt to form phases was strengthened, and as the EEV and absolute values of Gibbs free energies of ionic liquids increased, the ability of the salt to form phases also increased. The phase diagram was affected by temperature, and the binodal curves were right-shifted and absolute values of the tie-line slope decreased with increasing temperature.

ACKNOWLEDGEMENTS

This work was supported by the National Natural Science Foundation of China (No. 21606099), the Natural Science Foundation of Jilin Province (No. 20150520062JH and 20180623042TC) and Science and Technology Research Foundation of Jilin Province Department of Education (No. JJKH20170376KJ). We are grateful to Computing Center of Jilin Province for their essential support.

SUPPORTING INFORMATION

Additional information as noted in the text. This information is available via the Internet at http://www.springer.com/chemistry/journal/11814.

REFERENCES

1. L. Bulgariu and D. Bulgariu, *Sep. Purif. Technol.*, **80**, 620 (2011).
2. H. Li and X. J. Cao, *Process Biochem.*, **46**, 1753 (2011).
3. Z. G. Li, H. Teng and Z. L. Xiu, *Process Biochem.*, **46**, 586 (2011).
4. Y. M. Lu, W. J. Lu, W. Wang, Q. W. Guo and Y. Z. Yang, *Talanta*, **85**, 1621 (2011).
5. A. Salabat, R. Sadeghi, S. T. Moghadam and B. Jamehbozorg, *J. Chem. Thermodyn.*, **43**, 1525 (2011).
6. T. Furuya, Y. Iwai, Y. Tanaka, H. Uchida, S. Yamada and Y. Arai, *Fluid Phase Equilib.*, **103**, 119 (1995).
7. C. Grol3mann, R. Tintinger, J. Zhu and G. Maurer, *Fluid Phase Equilib.*, **106**, 111 (1995).
8. E. C. De Souza, R. S. Diniz, J. S. Dos Reis Coimbra, M. De Oliveira Leite, G. Rocha dos Santos, A. M. Da Cruz Rodrigues and L. H. Meller da Silva, *J. Chem. Eng. Data*, **58**, 2008 (2013).
9. R. S. Diniz, E. C. Souza, J. S. R. Coimbra, E. B. de Oliveira and A. R. da Costa, *J. Chem. Eng. Data*, **57**, 280 (2012).
10. J. Han, C. Yu, Y. Wang, X. Xie, Y. Yan, G. Yin and W. Guan, *Fluid Phase Equilib.*, **295**, 98 (2010).
11. C. Li, J. Han, Y. W. Wang, Y. Yan, J. Pan, X. Xu and Z. Zhang, *J. Chem. Eng. Data*, **55**, 1087 (2010).
12. C. Z. Sheng, J. Han, Y. Wang, B. Chen, Y. Liu, G. C. Zhang, Y. S. Yan and X. H. Zhao, *Fluid Phase Equilib.*, **364**, 55 (2014).
13. Y. C. Pei, J. J. Wang, L. Liu, K. Wu and Y. Zhao, *J. Chem. Eng. Data*, **52**, 2026 (2007).
14. M. T. Zafarani-Moattar, S. Hamzehzadeh and S. Nasiri, *Biotechnol. Prog.*, **28**, 146 (2012).
15. Y. Wang, X. Xu, Y. Yan, J. Han and Z. Zhang, *Thermochim. Acta*, **501**, 112 (2010).
16. X.-L. Wei, Z.-B. Wei, X.-H. Wang, Z.-N. Wang, D.-Z. Sun, J. Liu and H. H. Zhao, *Soft Matter*, **7**, 5200 (2011).
17. E. L. Cheluget, S. Marx, M. E. Weber and J. H. Vera, *J. Solution Chem.*, **23**, 275 (1994).
18. X. Yang, Y. Lu, Z. Sun, K. Cui and Z. Tan, *J. Chem. Eng. Data*, **63**, 625 (2018).
19. Y. Wang, S. P. Hu, J. Han and Y. S. Yan, *J. Chem. Eng. Data*, **55**, 4574 (2010).
20. Y. Wang, Y. Mao, J. Han, Y. Liu and Y. Yan, *J. Chem. Eng. Data*, **55**, 5621 (2010).
21. Y. Lu, J. Han, C. Z. Sheng, P. Yu, Z. J. Tan and Y. S. Yan, *Thermochim. Acta*, **543**, 1 (2012).
22. Y. Lu, J. Han, Z. J. Tan and Y. S. Yan, *J. Chem. Eng. Data*, **57**, 2313 (2012).
23. M. Perumalsamy and T. Murugesan, *J. Chem. Eng. Data*, **54**, 1359 (2009).
24. J. Han, Y. Wang, C. L. Yu, Y. F. Li, W. B. Kang and Y. S. Yan, *J. Chem. Thermodyn.*, **45**, 59 (2012).
25. Z. Y. Li, Y. C. Pei, L. Liu and J. J. Wang, *J. Chem. Thermodyn.*, **42**, 932 (2010).
26. P. Gonzalez-Tello, F. Camacho, G. Blazquez and F. J. Alarcon, *J. Chem. Eng. Data*, **41**, 1333 (1996).
27. J. Han, Y. Wang, Y. Li, C. Yu and Y. Yan, *J. Chem. Eng. Data*, **56**, 3679 (2011).
28. Y. H. Chen, Y. S. Meng, S. M. Zhang, Y. Zhang, X. W. Liu and J. Yang, *J. Chem. Eng. Data*, **55**, 3612 (2010).
29. Y. Lu, J. Han, Z. J. Tan and Y. S. Yan, *J. Chem. Eng. Data*, **58**, 118 (2013).
30. Y. Lu, T. F. Hao, M. Yan, J. Han, Z. J. Tan and Y. S. Yan, *J. Chem. Eng. Data*, **59**, 1843 (2014).
31. Y. Lu, T. F. Hao, Y. Zhou, J. Han, Z. J. Tan and Y. S. Yan, *J. Chem. Thermodyn.*, **71**, 137 (2014).
32. Y. Wang, S. P. Hu, Y. S. Yan and W. S. Guan, *CALPHAD*, **33**, 726 (2009).
33. M. T. Zafarani-Moattar and S. Hamzehzadeh, *J. Chem. Eng. Data*, **54**, 833 (2009).
34. Y. Guan, T. H. Lilley and T. E. Treffry, *Macromolecules*, **26**, 3971 (1993).
35. R. D. Rogers, A. H. Bond, C. B. Bauer, J. Zhang and S. T. Griffin, *J. Chromatogr. B*, **680**, 221 (1996).
36. M. T. Zafarani-Moattar and S. Hamzehzadeh, *J. Chem. Eng. Data*, **54**, 833 (2009).
37. R. Sadeghi and F. Ziamajidi, *Fluid Phase Equilib.*, **255**, 46 (2007).
38. R. Sadeghi and R. Golabiazar, *J. Chem. Eng. Data*, **55**, 74 (2010).
39. K. S. Nascimento, S. Yelo, B. S. Cavada, A. M. Azevedo and M. R. Aires-Barros, *J. Chem. Eng. Data*, **56**, 190 (2011).
40. Y. Wang, Y. S. Yan, S. P. Hu, J. Han and X. H. Xu, *J. Chem. Eng. Data*, **55**, 876 (2010).

Supporting Information

Measurement and correlation of phase equilibria in aqueous two-phase systems containing ionic liquid ([EOMiM]Br) and potassium citrate/ammonium citrate/potassium tartrate at different temperatures

Dongdong Wang[*,], Yang Lu[*,**,†], Zhuo Sun[*,**], Wei Liang[*,**], Dongshu Sun[*], Changli Qi[*], ChengZhuo Sheng[*], and Xiaopeng Yu[*,†]**

*Key Laboratory of Preparation and Application of Environmental Friendly Materials, Jilin Normal University, Ministry of Education, Changchun, 130103, China
**Jilin Provincial Key Laboratory for Numerical Simulation, Jilin Normal University, 1301 Haifeng Street, Siping, 136000, China
(*Received 12 July 2019 • accepted 24 November 2019*)

Table S1. Binodal data for the [EOMiM]Br(1)+$K_3C_6H_5O_7$(2)+H_2O(3) ATPSs at T=288.15, 298.15 and 308.15 K[a] and SD of Eqs. (5) and (6)

T=288.15 K		T=298.15 K		T=308.15 K	
$100w_1$	$100w_2$	$100w_1$	$100w_2$	$100w_1$	$100w_2$
58.75	0.55	58.89	0.93	60.46	1.23
56.83	1.31	57.14	1.52	58.05	2.13
55.08	2.02	56.10	2.01	57.00	2.51
53.89	2.51	54.78	2.56	55.63	3.01
52.13	3.25	52.75	3.48	55.06	3.36
50.32	4.03	50.01	4.57	53.72	3.72
48.11	5.01	48.01	5.52	51.61	4.57
47.40	5.33	46.01	6.39	50.24	5.24
45.80	6.07	44.50	7.14	48.31	6.02
44.85	6.52	41.06	8.94	47.20	6.38
43.38	7.23	39.34	9.72	45.59	7.23
41.73	8.05	37.73	10.88	43.33	8.16
40.73	8.56	36.06	11.65	41.16	9.23
39.62	9.14	34.10	12.88	38.99	10.57
37.45	10.32	32.65	13.97	36.66	11.84
35.99	11.15	31.68	14.71	35.06	12.96
33.64	12.56	30.35	15.54	33.07	14.13
31.83	13.72	29.27	16.35	31.88	15.28
28.50	16.08	27.32	17.93	30.36	16.56
27.00	17.28	25.03	19.74	28.03	18.36
SD_1[a]	SD_2[a]	SD_1[a]	SD_2[a]	SD_1[a]	SD_2[a]
0.49	0.49	0.27	0.18	0.28	0.34

[a]SD_1 was the SD for Eq. (5), SD_2 was the SD for Eq. (6). $SD=(\Sigma_{i=1}^{n}(w_1^{cal}-w_1^{exp})^2/N)^{0.5}$ where w_1^{exp} is the experimental mass fraction of [EOMiM]Br in this Tables, w_1^{cal} is the corresponding data calculated using Eq. (5) and Eq. (6). N represents the number of binodal data

Table S2. Binodal data for the [EOMiM]Br(1)+$(NH_4)_3C_6H_5O_7$/$K_2C_4H_4O_6$(2)+H_2O(3) ATPSs at T=308.15 K SD of Eqs. (5) and (6)

[EOMiM]Br-$(NH_4)_3C_6H_5O_7$ ATPS		[EOMiM]Br-$K_2C_4H_4O_6$ ATPS	
$100w_1$	$100w_2$	$100w_1$	$100w_2$
60.42	6.86	69.28	2.21
59.68	7.24	63.99	3.51
57.26	8.75	61.70	4.56
55.54	9.18	59.37	5.12
53.96	10.52	57.18	6.27
53.10	10.89	55.52	7.18
53.00	11.15	51.84	8.56
50.35	12.56	50.36	9.47
47.23	14.49	48.87	10.35
46.86	15.16	44.42	12.88
43.41	17.59	43.06	13.59
42.08	18.88	40.31	15.49
39.71	20.17	37.29	17.88
38.72	21.08	34.49	19.39
36.72	22.98	29.34	23.28
33.60	25.35	28.63	24.12
31.82	27.34	24.80	27.52
29.76	28.91	21.78	29.95
26.22	31.63	19.12	32.43
23.33	34.13	15.78	35.88
SD_1[a]	SD_2[a]	SD_1[a]	SD_2[a]
0.56	0.65	0.53	0.65

[a]SD_1 was the SD for Eq. (5), SD_2 was the SD for Eq. (6). $SD=(\Sigma_{i=1}^{n}(w_1^{cal}-w_1^{exp})^2/N)^{0.5}$ where w_1^{exp} is the experimental mass fraction of [EOMiM]Br in this Tables, w_1^{cal} is the corresponding data calculated using Eq. (5) and Eq. (6). N represents the number of binodal data

Uncertainty Calculation Method

The uncertainty was calculated by the follow equation:

$$\sigma=\sqrt{\frac{\Sigma_{i=1}^{n}(x_i-\bar{x})^2}{n(n-1)}}$$

where x represents sample value, i represents sample number, n represents sample size, $\bar{x}$ represents average value of sample values.